Tuning the Activity of Catechol Oxidase Model Complexes by Geometric Changes of the Dicopper Core

Jens Ackermann,[a, b] Franc Meyer,[a, b]* Elisabeth Kaifer,[a] and Hans Pritzkow[a]

Abstract: Dicopper(II) complexes of a series of different pyrazolate-based dinucleating ligands $[L^1]^- - [L^4]^-$ have been synthesized and characterized structurally and spectroscopically. A major difference between the four complexes is the individual metal–metal separation that is enforced by the chelating side arms of the pyrazolate ligand scaffold: it varies from 3.45 Å in $\mathbf{2}\cdot(BF_4)_4$ to 4.53 Å in $\mathbf{4}\cdot(ClO_4)_2$. All complexes have been evaluated as model systems for the catechol oxidase enzyme by using 3,5-di-*tert*-butylcatechole (DTBC) as the test substrate. They were shown to exhibit very different catecholase activities ranging from very efficient to poor catalysts (k_{obs} between 2430 ± 202 and $22.8 \pm 1.2\ h^{-1}$), with an order of decreasing activity $\mathbf{2}\cdot(ClO_4)_4 > \mathbf{1}\cdot(ClO_4)_2 > \mathbf{3}\cdot(ClO_4)_2 \gg \mathbf{4}\cdot(ClO_4)_2$. A correlation of the catecholase activities with the variation in Cu···Cu distances, as well as other effects resulting from the distinct redox potentials, neighboring groups, and the individual coordination spheres are discussed. Saturation behavior for the rate dependence on substrate concentration was observed in only two cases, that is, for the most active $\mathbf{2}\cdot(ClO_4)_4$ and for the least active $\mathbf{4}\cdot(ClO_4)_2$, whereas a catalytic rate that is almost independent of substrate concentration (within the range studied) was observed for $\mathbf{1}\cdot(ClO_4)_2$ and $\mathbf{3}\cdot(ClO_4)_2$. H_2O_2 was detected as the product of O_2 reduction in the catecholase reaction of the three most active systems. The structures of the adducts of "L^3Cu_2" and "L^4Cu_2" with a substrate analogue (tetrachlorocatecholate, TCC) suggest a bidentate substrate coordination to only one of the copper ions for those catalysts that feature short ligand side arms and correspondingly exhibit larger metal–metal separations; this possibly contributes to the lower activity of these systems. TCC binding is supported by several H-bonding interactions to water molecules at the adjacent copper or to ligand-side-arm N-donors; this emphasizes the importance of functional groups in proximity to the bimetallic active site.

Keywords: bimetallic complexes · bioinorganic chemistry · cooperative phenomena · copper · oxidation

Introduction

In the active sites of numerous metalloenzymes, two adjacent metal ions work cooperatively in order to achieve the transformation of substrate molecules.[1] This is particularly true for biological oxidase or oxygenase activity involving molecular oxygen, in which the metal ions serve to activate the kinetically inert O_2, and the combined redox power of the two metal ions is used to mediate and to control the multielectron redox reactions.[2, 3] In view of the great importance of oxidation reactions for industrial and synthetic processes and of the ongoing search for new and efficient oxidation catalysts, it is of paramount interest to elucidate the basic functional principles that govern such bimetallic reactivity of natural enzymes.

Dicopper sites play a pivotal role in biological oxygen chemistry and, consequently, the understanding of structural and functional aspects of copper metalloenzymes is a subject of intensive research.[3–7] A prominent member of these copper proteins is catechol oxidase, which features a type 3 center with two proximate copper ions in N-donor (histidine) ligation, and which catalyzes the two-electron oxidation of *ortho*-diphenols to the corresponding quinones (Scheme 1).[6, 7] The recent X-ray crystallographic characterization of catechol oxidase from sweet potatoes is a milestone in the field, revealing details of the enzyme structure in different redox states and in its complex with bound

[a] Priv.-Doz. Dr. F. Meyer, Dipl.-Chem. J. Ackermann, Dr. E. Kaifer, Dr. H. Pritzkow
Anorganisch-Chemisches Institut der Universität Heidelberg
Im Neuenheimer Feld 270, 69120 Heidelberg (Germany)
Fax: (+49) 6221-545707

[b] New address: Institut für Anorganische Chemie
Georg-August-Universität Göttingen
Tammannstr. 4, 37077 Göttingen (Germany)
E-mail: franc.meyer@chemie.uni-goettingen.de

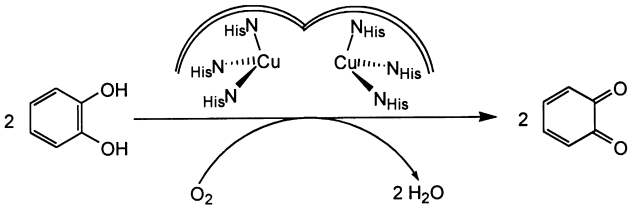

Scheme 1. Catecholase reaction.

 © WILEY-VCH Verlag GmbH, 69451 Weinheim, Germany, 2002 0947-6539/02/0801-0247 $ 17.50+.50/0

inhibitor.[7] Based on these structural findings as well as on previous spectroscopic and biochemical evidence, a plausible mechanism has been proposed for the catecholase activity.[7] This mechanism includes activation of O_2 as a peroxide bound to both copper ions, and it allows the two-electron substrate oxidation to occur by means of the cooperative action of the two copper ions, as each individual copper ion only undergoes a one-electron redox shuttle between the +I and +II states during turnover.

Quite a number of mono- and dinuclear copper coordination compounds have been investigated as biomimetic catalysts for catechol oxidation.[8–13] While no clear relation between the catalytic activity and the redox potential of the copper species has emerged,[9] dinuclear copper complexes are generally found to be more reactive than mononuclear compounds, and a steric match between the dicopper site and the substrate is assumed to be advantageous.[10, 11] Some correlations between the observed rates of reactivity and ligand architecture, copper coordination environment, or preorganization of the metal ions have been observed for particular classes of complexes.[12] However, a more general understanding of structure–reactivity patterns that might allow for a rational design of catalytically most active copper complexes is still lacking. Further studies of well defined and tunable dicopper complexes are obviously needed to gain deeper insight into these copper-mediated substrate oxidations and to finally unravel the parameters that determine bimetallic reactivity both in natural metalloenzymes and in small synthetic catalysts.

In this contribution, we report a series of closely related yet distinct dicopper(II) complexes that are based on multifunctional pyrazolate ligands. The various ligand scaffolds differ by the number of N-donor sites and by the length of the chelating side arms attached to the heterocycle (Scheme 2).[14] These variations have previously been shown to enable a tuning of the preorganization of the bimetallic framework, in particular with respect to the metal–metal separation.[15] The properties of the new dicopper complexes are described and their catecholase activity is studied. Some adducts with tetrachlorocatechol are examined to model possible modes of substrate binding to the bimetallic core.

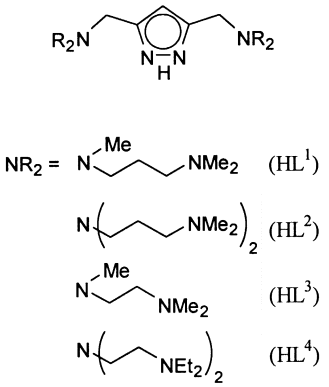

Scheme 2. Ligands used in this work.

Results and Discussion

Synthesis and structural characterization of the complexes: Dicopper(II) complexes of pyrazolate ligands $[L^1]^-$, $[L^2]^-$, $[L^3]^-$, and $[L^4]^-$ were prepared, and their crystal structures determined. Schematic representations of the complexes are depicted in Scheme 3 (in the case of **1**, the analogous complex **1′**, which bears ethanol instead of methanol ligands was analyzed crystallographically). Molecular structures of the cations as revealed by X-ray crystallography are shown in Figures 1–4 together with selected atom distances and bond angles.

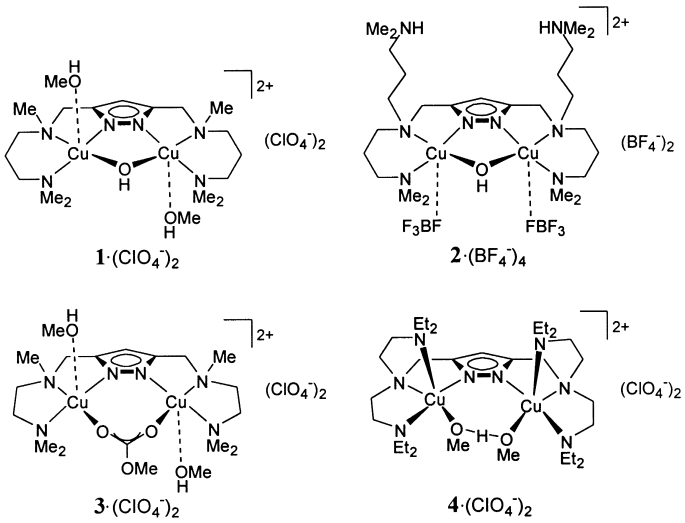

Scheme 3. Dinuclear copper(II) complexes of the various pyrazolate ligands.

In all cases, the copper(II) ions are nested within their respective coordination compartments and are spanned by

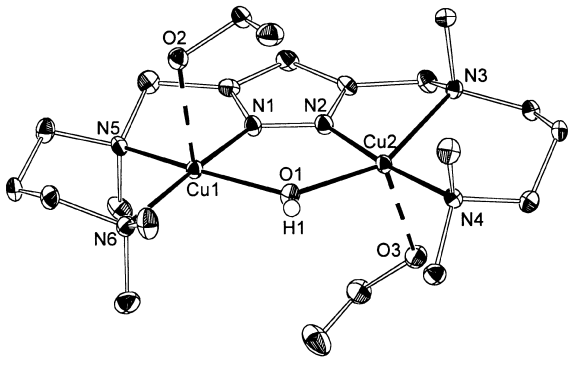

Figure 1. Molecular Structure of **1′** (40% probability ellipsoids). All hydrogen atoms except H1 have been omitted for clarity. Selected atom distances [Å] and bond angles [°]: Cu1–N1 1.883(2), Cu1–N6 2.008(2), Cu1–O1 2.026(2), Cu1–N5 2.181(2), Cu1–O2 2.321(2), Cu2–N2 1.885(2), Cu2–N4 1.999(2), Cu2–O1 2.024(2), Cu2–N3 2.170(2), Cu2–O3 2.364(2), Cu1···Cu2 3.540(1); N1-Cu1-N6 170.65(9), N1-Cu1-O1 82.99(9), N6-Cu1-O1 101.64(9), N1-Cu1-N5 76.88(9), N6-Cu1-N5 96.76(9), O1-Cu1-N5 156.66(9), N1-Cu1-O2 91.10(9), N6-Cu1-O2 96.27(9), O1-Cu1-O2 97.53(8), N5-Cu1-O2 94.59(8), N2-Cu2-N4 174.5(1), N2-Cu2-O1 83.19(9), N4-Cu2-O1 101.03(8), N2-Cu2-N3 77.10(9), N4-Cu2-N3 97.80(9), O1-Cu2-N3 154.11(8), N2-Cu2-O3 88.09(9), N4-Cu2-O3 94.04(8), O1-Cu2-O3 106.68(9), N3-Cu2-O3 89.42(9).

© WILEY-VCH Verlag GmbH, 69451 Weinheim, Germany, 2002
0947-6539/02/0801-0248 $ 17.50+.50/0 *Chem. Eur. J.* **2002**, *8*, No. 1

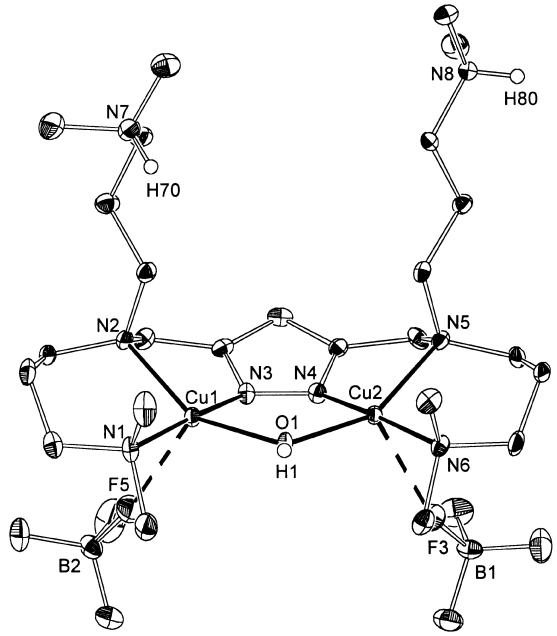

Figure 2. Molecular Structure of $\mathbf{2}\cdot(BF_4)_2$ (30% probability ellipsoids). All hydrogen atoms except the H1, H70, and H80 have been omitted for clarity. Selected atom distances [Å] and bond angles [°]: Cu1–N3 1.896(6), Cu1–N1 1.995(7), Cu1–O1 1.999(5), Cu1–N2 2.147(6), Cu1–F5 2.487(8), Cu2–N4 1.896(6), Cu2–O1 1.991(5), Cu2–N6 2.013(6), Cu2–N5 2.127(6), Cu2–F3 2.603(6), Cu1···Cu2 3.447(2); N3-Cu1-N1 173.8(3), N3-Cu1-O1 85.5(2), N1-Cu1-O1 97.5(2), N3-Cu1-N2 79.4(2), N1-Cu1-N2 100.0(2), O1-Cu1-N2 151.1(2), O1-Cu1-F5 118.2(9), N1-Cu1-F5 85.9(4), N2-Cu1-F5 85.9(3), N3-Cu1-F5 87.8(3), N4-Cu2-O1 85.5(2), N4-Cu2-N6 174.1(2), O1-Cu2-N6 97.3(3), N4-Cu2-N5 79.7(2), O1-Cu2-N5 153.2(2), N6-Cu2-N5 99.6(3), O1-Cu2-F3 113.4(3), N4-Cu2-F3 88.0(3), N5-Cu2-F3 88.3(3), N6-Cu2-F3 86.0(3).

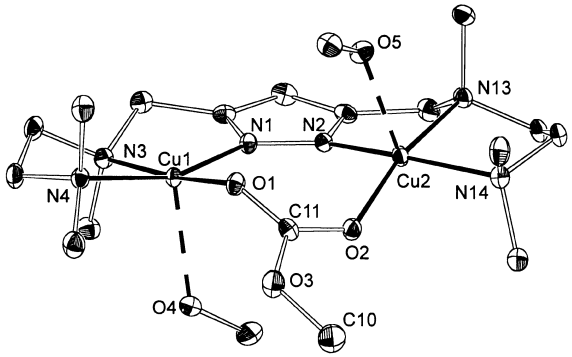

Figure 3. Molecular Structure of **3** (40% probability ellipsoids). All hydrogen atoms have been omitted for clarity. Selected atom distances [Å] and bond angles [°]: Cu1–N1 1.918(2), Cu1–O1 1.971(2), Cu1–N4 2.029(2), Cu1–N3 2.069(2), Cu1–O4 2.306(2), Cu2–N2 1.947(2), Cu2–O2 1.966(2), Cu2–N14 2.060(2), Cu2–N13 2.064(2), Cu2–O5 2.328(2), Cu1···Cu2 4.088(1); N1-Cu1-O1 99.09(8), N1-Cu1-N4 160.45(8), O1-Cu1-N4 89.81(8), N1-Cu1-N3 82.46(9), O1-Cu1-N3 173.06(8), N4-Cu1-N3 86.74(9), N1-Cu1-O4 97.83(8), O1-Cu1-O4 88.33(7), N4-Cu1-O4 99.81(8), N3-Cu1-O4 98.19(8), N2-Cu2-O2 101.15(8), N2-Cu2-N14 163.42(9), O2-Cu2-N14 89.14(8), N2-Cu2-N13 81.69(9), O2-Cu2-N13 168.74(8), N14-Cu2-N13 85.81(9), N2-Cu2-O5 93.82(8), O2-Cu2-O5 93.12(8), N14-Cu2-O5 98.61(8), N13-Cu2-O5 97.58(8).

the bridging pyrazolate moiety. Each copper atom in complexes $\mathbf{1'}\cdot(ClO_4)_2$, $\mathbf{2}\cdot(BF_4)_4$, and $\mathbf{3}\cdot(ClO_4)_2$ is in a roughly square-planar coordination environment consisting of three N-donors from the chelating pyrazolate ligand and an O atom

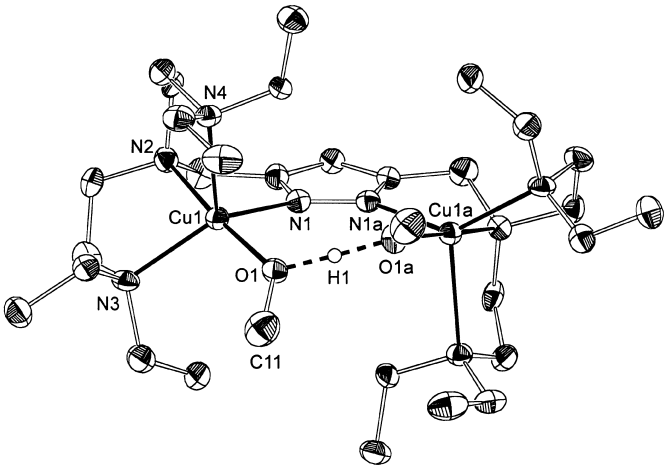

Figure 4. Molecular Structure of **4** (30% probability ellipsoids). All hydrogen atoms except H1 have been omitted for clarity. Selected atom distances [Å] and bond angles [°]: Cu1–O1 1.943(4), Cu1–N2 2.040(5), Cu1–N1 2.057(5), Cu1–N3 2.129(6), Cu1–N4 2.336(5), Cu1···Cu1a 4.553(1), O1···O1a 2.400(9); O1-Cu1-N2 173.9(2), O1-Cu1-N1 92.3(2), N2-Cu1-N1 81.8(2), O1-Cu1-N3 101.6(2), N2-Cu1-N3 84.0(2), N1-Cu1-N3 135.7(2), O1-Cu1-N4 97.8(2), N2-Cu1-N4 82.2(2), N1-Cu1-N4 104.9(2), N3-Cu1-N4 114.4(2).

from a secondary bridging unit located within the bimetallic pocket. An additional axial position is occupied by a solvent molecule (**1′**, **3**) or counter anion (**2**) at a greater distance, typical for Jahn–Teller distortion.

As expected for the long ligand side arms of $[L^1]^-$, a comparatively short metal–metal distance is found in **1′** [3.540(1) Å].[15] During the synthesis of $\mathbf{1}\cdot(ClO_4)_2$, two equivalents of an external base have to be added to achieve reasonable yields: one equivalent serves to deprotonate the pyrazole NH, the second provides the hydroxide secondary bridge. In the case of $[L^2]^-$, in which further long side arms are attached to the heterocycle, the two additional N-functions within these side arms now act as an internal base to capture the two protons that are liberated upon complexation. Thus, the resulting dinuclear frameworks are quite similar in both **1′** and **2**, and also have comparable metal–metal distances [3.447(2) Å in **2**]. The major difference is the extra ammonium groups in close proximity to the bimetallic core of **2**. Further characteristics of the solid state structures of $\mathbf{1'}\cdot(ClO_4)_2$ and $\mathbf{2}\cdot(BF_4)_4$ are as follows: in **1′**, the proton of the hydroxide forms a weak bridge to one of the perchlorate counter anions [$d(O1\cdots O13_{ClO_4}) = 3.319$ Å], and the protons of the ethanol solvent molecules have been located H-bridging to perchlorate O-atoms [$d(O2\cdots O14_{ClO_4}) = 2.792$ Å, $d(O3\cdots O10_{ClO_4}) = 2.844$ Å]. The two copper ions are located approximately within the plane defined by the pyrazolate heterocycle (displacement out of the plane: 0.09 Å for Cu1, 0.13 Å for Cu2), and the equatorial coordination planes of the copper ions are only slightly tilted with respect to each other (5.3°) and with respect to the pyrazolate (8.3° and 8.7°). In $\mathbf{2}\cdot(BF_4)_4$, the OH and NH protons likewise form hydrogen bridges to BF_4^- counteranions [$d(O1\cdots F12) = 3.033$ Å, $d(N7\cdots F9) = 2.887$ Å, $d(N8\cdots F4/F13) = 2.953/2.846$ Å]. However, the copper ions in $\mathbf{2}\cdot(BF_4)_4$ are more severely displaced out of the plane defined by the pyrazolate (0.70 Å

for Cu1, 0.73 Å for Cu2), and the equatorial coordination planes of the copper ions are drastically tilted with respect to each other (28.3°) and with respect to the pyrazolate (17.9° and 18.8°).

The shorter ligand side arms in $[L^3]^-$ are known to pull the metal ions back and apart, thus preventing copper–copper distances short enough to allow for a bridging binding mode of a small hydroxide within the bimetallic pocket.[15] The coordination compound first formed in the reaction of HL^3 with two equivalents of $Cu(ClO_4)_2$ and two equivalents of base was found to gradually absorb CO_2 from air, yielding complex $\mathbf{3}\cdot(ClO_4)_2$ in methanol solution (Scheme 3). Compound **3** features a methyl carbonate bridge (as confirmed by a strong IR absorption at 1612 cm^{-1}) and an increased metal–metal separation of 4.088(1) Å. The carbonate plane is drastically tilted with respect to the pyrazolate plane (33.6°), and also the basal coordination planes of the two copper ions are severely tilted with respect to each other (25.3°). This suggests a considerably strained situation after incorporation of the carbonate bridge within the bimetallic pocket, which should facilitate subsequent replacement of the carbonate by other ligands or substrates. FAB MS spectra support this assumption, because dominant signals at $m/z = 421$ and 520, corresponding to the carbonate-devoid ions $[L^3Cu_2]^+$ and $[L^3Cu_2(ClO_4)]^+$, appear besides the less intense parent signal for $[L^3Cu_2(ClO_4)(CH_3OCO_2)]^+$ ($m/z = 595$). Formation of **3** can be accelerated by bubbling CO_2 through the reaction mixture. As the catecholase reaction catalyzed by the new copper complexes was intended to be carried out in methanol with air as the oxidant (see below), complex $\mathbf{3}\cdot(ClO_4)_2$ prepared in such a way was employed to ensure the use of a well-defined dicopper precatalyst in all subsequent experiments.

Ligand $[L^4]^-$ bears additional short side arms. In $\mathbf{4}\cdot(ClO_4)_2$, these are coordinated to the metal ions, and thus the metal ions are pulled apart even more, and the metal–metal separation is further increased to 4.533(1) Å. The copper ions in **4** are five-coordinate with coordination polyhedra intermediate between square pyramidal and trigonal bipyramidal ($\tau = 0.64$).[16] Again, the enforced copper–copper distance is too large to allow for a bridging position of a one-atom O-bridge like hydroxide (or methoxide), but in this case incorporation of an additional solvent molecule (methanol) is observed to give an intramolecular MeO-H-OMe bridging unit featuring a very short hydrogen bridge [$d(O1\cdots O1a) = 2.400(9)$ Å]. Such units within the bimetallic pocket have previously been proven to be rather labile and to be susceptible to replacement by various other ligating molecules, for example by an incoming substrate.[15] Accordingly, the MeO-H-OMe group that is formed when the complex is crystallized from dry methanol undergoes facile exchange by water, and a HO-H-OH bridging moiety results from storage of $\mathbf{4}\cdot(ClO_4)_2$ in air or from recrystallizing the complex in wet methanol.

Spectroscopic and electrochemical properties of the complexes: UV/Vis spectra of the perchlorate salts of **1**–**4** have been recorded in methanol (Table 1). All complexes show strong absorptions around 218 and 270 nm, which are assigned to pyrazolate $\pi-\pi^*$ and metal-to-ligand charge transfer transitions. Weak Cu^{II} ligand field bands appear at 621, 589, and 638 nm for **1**, **2**, and **3**, respectively. These band positions are in accordance with elongated tetragonal or square-pyramidal coordination,[17] as observed in the crystal structures. In contrast, complex **4** shows a broad $d-d$ absorption centered at 855 nm and suggestive of trigonal-bipyramidal coordination including four N donors of the $[L^4]^-$ ligand for each copper ion, similar to the solid state situation. Diffuse reflectance spectra of solid samples of the perchlorate salts display the same trends, that is, $d-d$ bands in the range 630–680 nm for **1**–**3** versus a broad low-energy absorption around 1020 nm for **4**; this indicates that the overall structural features as elucidated by X-ray crystallography are basically retained in solution.

Table 1. UV/Vis data of the complexes in methanol and in the solid state (diffuse reflectance); λ [nm] (ε [$M^{-1}cm^{-1}$]).

	methanol solution	diffuse reflectance
$\mathbf{1}\cdot(ClO_4)_2$	218 (7280), 267 (11010), 621 (210)	434 (sh), 682, 1420
$\mathbf{2}\cdot(ClO_4)_4$	218 (7410), 267 (9330), 375 (1710, sh) 589 (270)	418, 634, 1416
$\mathbf{3}\cdot(ClO_4)_2$	216 (7720), 271 (10930), 638 (280)	326, 658, 1424
$\mathbf{4}\cdot(ClO_4)_2$	219 (8790), 289 (7710), 855 (530)	376, 1020
$\mathbf{5}\cdot(ClO_4)_2$	225 (24320), 255 (13050), 300 (10260), 887 (360)	
$\mathbf{6}\cdot(ClO_4)_2$	227 (13960), 247 (13790), 303 (7670, sh), 629 (240)	
$\mathbf{7}\cdot PF_6$	200 (14370, sh), 223 (37870), 257 (14600), 299 (7600, sh), 476 (170), 618 (200)	

The electrochemical behavior of the perchlorate salts of **1**–**4** has been studied in MeCN by cyclic voltammetry. The results are summarized in Table 2. All complexes reveal only ill-defined anodic processes at high potentials (above +1.4 V versus the saturated calomel electrode) and irreversible reduction peaks. The latter are observed in the narrow range −0.30 to −0.38 V for **1**–**3** and at −0.51 V for **4** (at 200 mV s^{-1}). In the case of **2** (see Figure 5) and **3**, a second wave is found that peaks at −0.70 and −0.65 V, respectively, while further cathodic processes are ill-defined for **1** and **4**. The first reduction is assumed to involve formation of the Cu^ICu^I species in all cases (a shoulder at around −0.1 V at the first reduction peak of **2** might indicate a closely spaced two-step process, see Figure 5), while the second reduction for **2** presumably corresponds to Cu^0 release as indicated by the appearance of the anodic stripping of the electrodeposed Cu^0 in the back scan.[18] It is well established that O-containing bridges like HO^-, MeO^-, or carbonate have a very poor ability to bind to Cu^I centers and tend to dissociate from the

Table 2. Electrochemical properties of the complexes in acetonitrile (0.1 M $NnBu_4PF_6$, 200 mV s^{-1}); peak potentials in V vs. SCE.

	$E_p^{red,1}$	$E_p^{red,2}$	E_p^{ox}
$\mathbf{1}\cdot(ClO_4)_2$	−0.37	–	+1.52
$\mathbf{2}\cdot(ClO_4)_4$	−0.30	−0.70	+1.67
$\mathbf{3}\cdot(ClO_4)_2$	−0.38	−0.65	+1.46
$\mathbf{4}\cdot(ClO_4)_2$	−0.51	–	+1.63

© WILEY-VCH Verlag GmbH, 69451 Weinheim, Germany, 2002
0947-6539/02/0801-0250 $ 17.50+.50/0 *Chem. Eur. J.* **2002**, *8*, No. 1

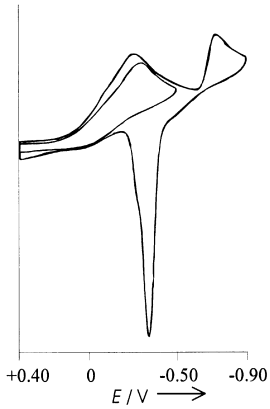

Figure 5. Cyclic voltammogram of complex $\mathbf{2}\cdot(ClO_4)_2$ recorded on a platinum electrode in MeCN containing $NnBu_4PF_6$ (0.1M) at scan speed 200 mV s^{-1}; potentials versus the saturated calomel electrode.

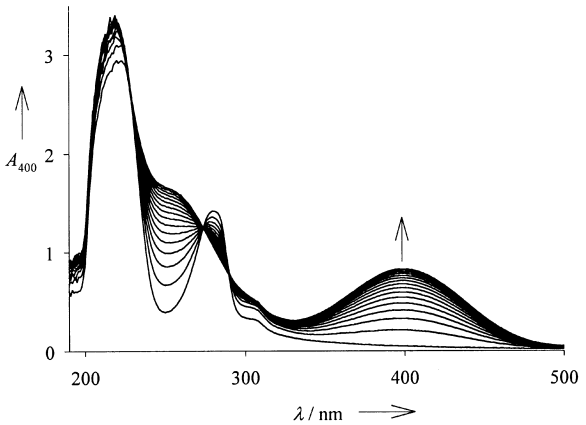

Figure 6. UV/Vis spectra of the course of the oxidation of 3,5-DTBC by $\mathbf{4}\cdot(ClO_4)_2$.

coordination sphere upon electrogeneration of the reduced metal species.[12, 18, 19] Furthermore, Cu^{II} and Cu^{I} show distinct preferences for different coordination polyhedra, and pronounced changes in coordination geometry are thus expected to occur, with the structures of the dicopper(I) species differing significantly from those determined for the dicopper(II) complexes. However, as pointed out previously,[12] this does by no means preclude the use of these bimetallic systems as oxidation catalysts.

Catecholase activity: 3,5-Di-*tert*-butylcatechol (3,5-DTBC) has been widely used as a substrate in catecholase model studies[8–13] and was also employed here. Its low redox potential makes it easy to oxidize,[20] and the bulky substituents prevent further reactions such as ring opening. The product, 3,5-di-*tert*-butylquinone (3,5-DTBQ), is sufficiently stable and displays a strong absorption at $\lambda_{max} = 400$ nm ($\varepsilon = 1684\,M^{-1}cm^{-1}$) whose appearance was monitored by UV/Vis spectroscopy in the kinetic studies. Reactivity studies were performed in methanol by using atmospheric oxygen, and the perchlorate salts were employed in all cases to ensure comparability without any interfering effects of different anions.

Initial qualitative experiments revealed drastic differences in activity for the four different complexes: while $\mathbf{1}\cdot(ClO_4)_2$ and $\mathbf{2}\cdot(ClO_4)_4$ exhibit very high catecholase activity, $\mathbf{3}\cdot(ClO_4)_2$ is somewhat less active, and substrate conversion by $\mathbf{4}\cdot(ClO_4)_2$ is significantly slower. The course of oxidation of 3,5-DTBC by $\mathbf{4}\cdot(ClO_4)_2$ with the increase in quinone absorption is shown in Figure 6. NMR spectroscopy of the product mixtures obtained from complete oxidation of ten equivalents of 3,5-DTBC confirmed the presence of 3,5-DTBQ as the sole product in all cases.

The kinetics of the catecholase model reactions were determined by the method of initial rates. With a large initial excess of the substrate, a linear dependence of the initial rates on the complex concentration was obtained (Figure 7); this is in accordance with the idea that two cooperating copper ions

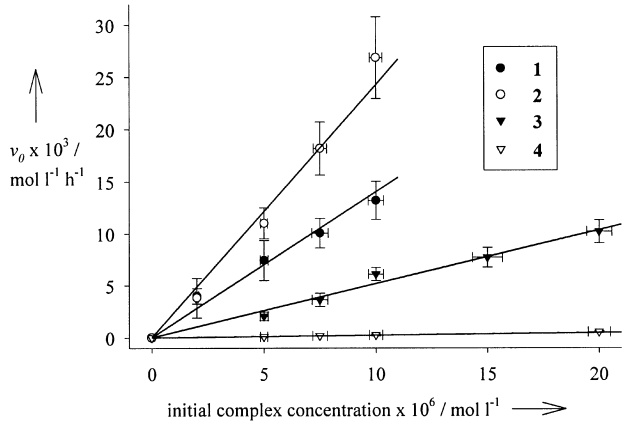

Figure 7. Effect of catalyst concentration on the initial rate of 3,5-DTBC oxidation (as measured by the absorbance change at 400 nm) by complexes $\mathbf{1}\cdot(ClO_4)_2$, $\mathbf{2}\cdot(ClO_4)_4$, $\mathbf{3}\cdot(ClO_4)_2$, and $\mathbf{4}\cdot(ClO_4)_2$ in methanol. The initial concentration of the substrate was 10^{-3}M.

are required to accomplish the two-electron oxidation of a catechol substrate molecule. The pseudo-first-order rate constants k_{obs} are collected in Table 3 and are taken as a first measure for comparing individual activities. Those two systems in which the longer ligand side arms allow for a shorter Cu···Cu separation are the most active, and it appears as if activity is correlated to the metal–metal distance. In particular, complex $\mathbf{2}\cdot(ClO_4)_4$ is a very effective catalyst for

Table 3. Kinetic parameters for the oxidation of 3,5-DTBC, and Cu···Cu separation of the catalyst complexes.

	k_{obs} [h^{-1}]	d(Cu···Cu) [Å]	k_{cat} [h^{-1}][a]	K_M [mol^{-1}L^{-1}][a]	v_{max} [mol^{-1}L^{-1}min^{-1}][a]
$\mathbf{1}\cdot(ClO_4)_2$	1400 ± 200	3.54	–	–	–
$\mathbf{2}\cdot(ClO_4)_4$	2430 ± 202	3.45	2804 ± 388	$(8.9 \pm 3.5) \times 10^{-5}$	$(4.7 \pm 0.6) \times 10^{-4}$
$\mathbf{3}\cdot(ClO_4)_2$	514 ± 70	4.09	–	–	–
$\mathbf{4}\cdot(ClO_4)_2$	22.8 ± 1.2	4.53	31.6 ± 11.3	$(7.9 \pm 4.0) \times 10^{-4}$	$(5.3 \pm 1.9) \times 10^{-6}$

[a] Determined from a Lineweaver–Burke plot.

 © WILEY-VCH Verlag GmbH, 69451 Weinheim, Germany, 2002 0947-6539/02/0801-0251 $ 17.50+.50/0

the catecholase reaction, not only within the present series, but also in comparison with most other catecholase model systems described previously.[8–13]

To gain further insight, the variation of the rates with the substrate concentrations was investigated. Unfortunately, due to their very high activities, no reliable data at substrate/catalyst ratios lower than 10 could be obtained for complexes **1**·$(ClO_4)_2$, **2**·$(ClO_4)_4$ and **3**·$(ClO_4)_2$ by our conventional UV/Vis technique (i.e., without stopped-flow equipment). The experimental results for all four systems are depicted in Figure 8 and reveal saturation behavior in the case of

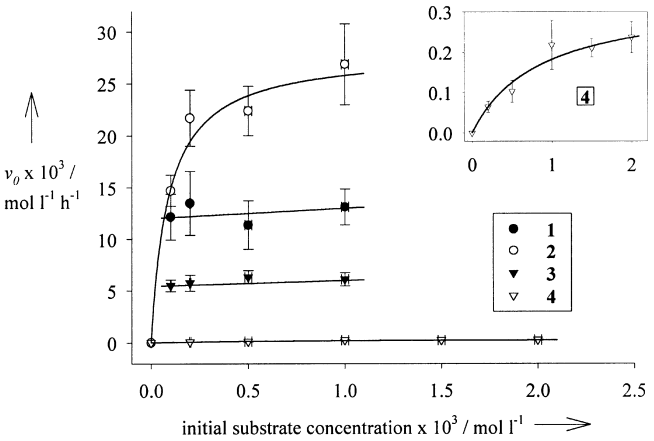

Figure 8. Effect of substrate concentration on the initial rate of 3,5-DTBC oxidation (as measured by the absorbance change at 400 nm) by complexes **1**·$(ClO_4)_2$, **2**·$(ClO_4)_4$, **3**·$(ClO_4)_2$, and **4**·$(ClO_4)_2$ in methanol. Concentration of the catalyst complex was 10^{-5} M.

complexes **2**·$(ClO_4)_4$ and **4**·$(ClO_4)_2$. A Michaelis–Menten analysis of these data sets was thus applied, from which we inferred that there is formation of a complex–substrate adduct as a pre-equilibrium process and irreversible formation of the quinone product and the free dicopper(I) species as the rate-determining step. This approach provides an estimation of K_M and k_{cat} values as determined from a Lineweaver–Burke plot and listed in Table 3 (the latter being reasonably consistent with the k_{obs} values given in the same table). It should be noted, though, that such a simplified model most certainly is not a fully appropriate description of the present systems, and that a more complicated mechanism may well be in effect, which furthermore may be distinct for each of the four catalyst complexes. The rate for complexes **1**·$(ClO_4)_2$ and **3**·$(ClO_4)_2$ turned out to be almost independent of 3,5-DTBC concentration within the range of substrate concentration studied. This is possibly due to a particularly high binding constant, but it might also indicate that a different step of the overall catalytic cycle is rate determining, for example the reoxidation of the dicopper(I) species by dioxygen.

Two sets of experiments were carried out to determine the fate of the O_2 oxidant, that is, whether hydrogen peroxide or water is formed as the reduced oxygen species (path A versus path B in Scheme 4). In the first experiments that were carried out with **1**·$(ClO_4)_2$, **2**·$(ClO_4)_4$, and **3**·$(ClO_4)_2$, methanol saturated with atmospheric oxygen was employed, and the

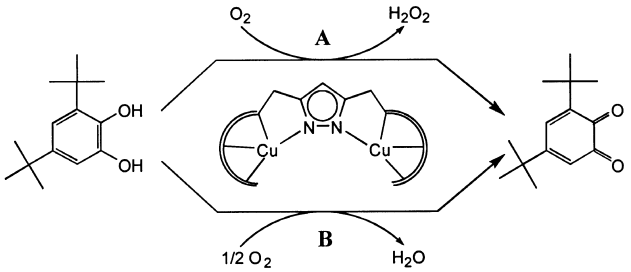

Scheme 4. Possible pathways for quinone formation.

reaction vessel closed air-tight immediately after mixing of the reactant solutions (10^{-4} M in complex and 5×10^{-3} M in substrate). Increase of the 400 nm band characteristic of quinone formation was then followed until the reaction had come to an end. Considering the solubility of O_2 in methanol under standard conditions (2.5×10^{-3} mol L^{-1})[21] and assuming that all the O_2 had been consumed at this point, an absorption of 0.8 was to be expected for a reaction stoichiometry according to path A, while an absorption of 1.6 would result from path B. The reaction vessel was then briefly opened, and air was bubbled into the solution. Renewed increase of the 400 nm absorption confirmed that the catalysts were still active and that full consumption of O_2 was indeed the cause for the catalytic reaction to stop. As an example, the results for **1**·$(ClO_4)_2$ are shown in Figure 9. As in the case of **2**·$(ClO_4)_4$ and **3**·$(ClO_4)_2$, the experimental findings strongly suggest the formation of H_2O_2 as the major product of O_2 reduction. Accumulation of H_2O_2 during turnover was then confirmed in a second set of experiments by means of the lactoperoxidase-accelerated I_3^- assay.[13, 22] 71%, 63%, and 58% of the expected amount of H_2O_2 were detected for **1**·$(ClO_4)_2$, **2**·$(ClO_4)_4$, and **3**·$(ClO_4)_2$, respectively.

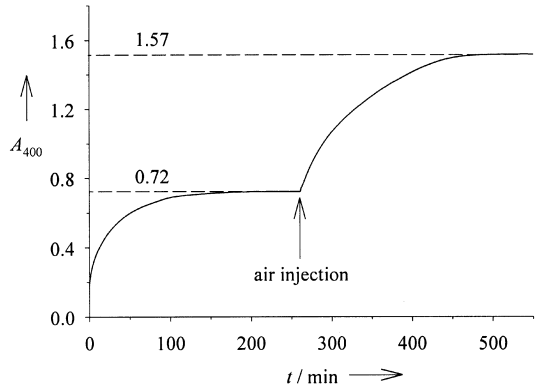

Figure 9. Time course of 3,5-DTBC oxidation (as measured by the absorbance change at 400 nm) by complex **1**·$(ClO_4)_2$ in methanol upon repeated purging with air. Initial concentrations of the catalyst and the substrate were 10^{-4} M and 5×10^{-3} M.

In the case of **4**·$(ClO_4)_2$, the I_3^- assay was only slightly different from a blank experiment. It remains uncertain at the present stage whether this is due to a different mechanism or has to be attributed to gradual decomposition of the initially formed H_2O_2 (possibly catalyzed by the complex) during the much longer reaction times required for the least active system **4**·$(ClO_4)_2$.

© WILEY-VCH Verlag GmbH, 69451 Weinheim, Germany, 2002
0947-6539/02/0801-0252 $ 17.50+.50/0 *Chem. Eur. J.* **2002**, *8*, No. 1

TCC complexes as models for substrate binding: To examine possible modes of substrate binding at the dicopper cores and to obtain structural information on the putative dicopper(II)-catecholate intermediate formed during the catalytic reaction, tetrachlorocatechol ($TCCH_2$) was employed as a mimic of the DTBC substrate. $TCCH_2$ is less prone to oxidation,[20] and may therefore form stable adducts with the copper(II) catalyst complexes. While several mononuclear copper complexes with bound catecholate are known,[23] only few structurally characterized *di*copper systems with coordinated TCC have hitherto been reported.[11] In the first of these compounds (reported by Karlin et al.),[11a] the TCC bridges two copper(II) ions at a rather short metal–metal separation of 3.248 Å. The original assumption that such bidentate substrate binding might also occur within the active site of catechol oxidase has recently been called into question by crystallographic findings for the native enzyme; these suggested an alternative mechanism with monodentate binding of the catechol to only one of the copper ions.[7]

Green crystalline material could be obtained from the reaction of **3**·$(ClO_4)_2$ and **4**·$(ClO_4)_2$ with $TCCH_2$ (Scheme 5),

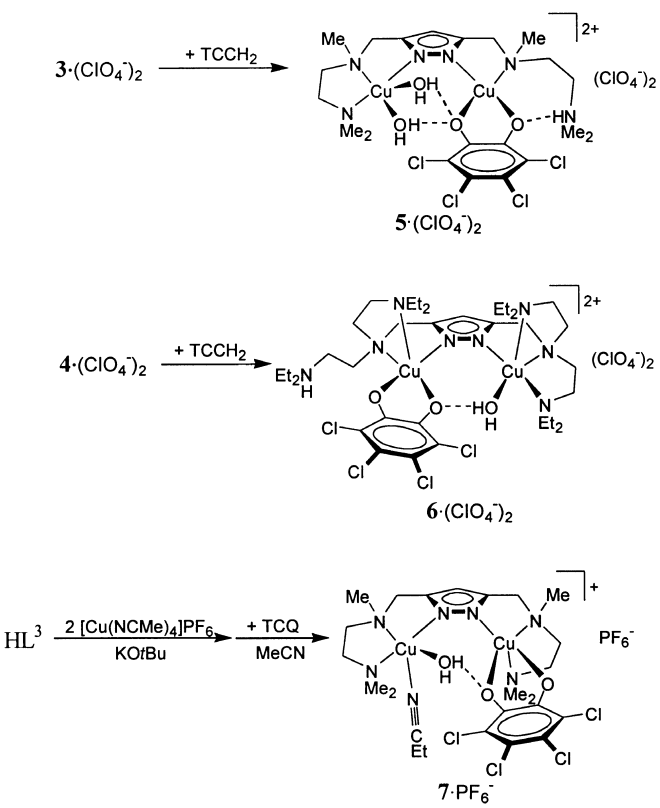

Scheme 5. Synthesis of TCC adducts **5**·$(ClO_4)_2$, **6**·$(ClO_4)_2$ and **7**·PF_6.

and the identity of these complexes was analyzed by X-ray crystallography. Molecular structures of the cations $[HL^3Cu_2(TCC)(H_2O)_2]^{2+}$ (**5**) and $[HL^4Cu_2(TCC)(H_2O)]^{2+}$ (**6**) are depicted in Figures 10 and 11, respectively, including one of the ClO_4^- counteranions in the former case.

Complex **6**·$(ClO_4)_2$ is found to contain two independent but quite similar molecular entities per unit cell. Molecular structures of the TCC adducts of the dicopper framework are

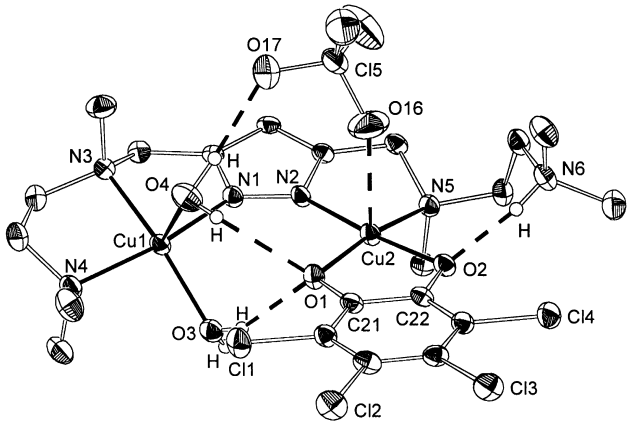

Figure 10. Molecular Structure of **5** (30% probability ellipsoids). All hydrogen atoms except the N- and O-bound hydrogen atoms have been omitted for clarity. Selected atom distances [Å] and bond angles [°]: Cu1–N1 1.941(3), Cu1–O3 2.015(3), Cu1–N4 2.028(3), Cu1–N3 2.043(3), Cu1–O4 2.298(3), Cu2–O2 1.933(2), Cu2–O1 1.934(2), Cu2–N2 1.944(3), Cu2–N5 2.083(3), O1–C21 1.339(4), O2–C22 1.344(4), C21–C22 1.412(5), Cu2–O16 2.666(1), N6···O2 2.655(4), O3···O1 2.614(4), O4···O1 2.994(4), O4···O17 2.960(3), Cu1···Cu2 4.202(1); N1-Cu1-O3 96.8(1), N1-Cu1-N4 165.8(1), O3-Cu1-N4 92.5(1), N1-Cu1-N3 81.7(1), O3-Cu1-N3 165.0(1), N4-Cu1-N3 86.5(1), N1-Cu1-O4 92.3(1), O3-Cu1-O4 92.7(1), N4-Cu1-O4 97.9(1), N3-Cu1-O4 102.2(1), O2-Cu2-O1 85.56(9), O2-Cu2-N2 174.7(1), O1-Cu2-N2 98.9(1), O2-Cu2-N5 95.2(1), O1-Cu2-N5 169.4(1), N2-Cu2-N5 80.9(1).

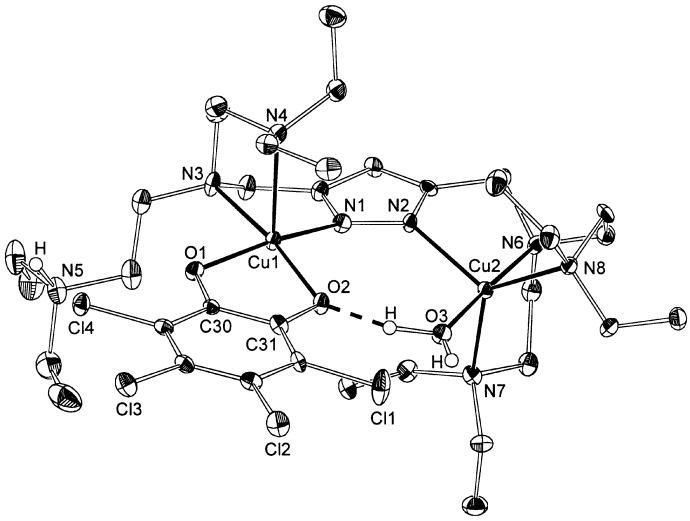

Figure 11. Molecular Structure of **6** (30% probability ellipsoids). All hydrogen atoms except the N- and O-bound hydrogen atoms have been omitted for clarity. Selected atom distances [Å] and bond angles [°] (values for the second independent molecules are given in parentheses): Cu1–O1 1.918(3) [1.939(3)], Cu1–N1 1.972(4) [1.974(4)], Cu1–O2 1.979(3) [1.984(3)], Cu1–N3 2.127(4) [2.110(4)], Cu1–N4 2.423(4) [2.358(4)], Cu2–O3 1.949(4) [1.951(4)], Cu2–N6 2.032(4) [2.049(4)], Cu2–N2 2.095(4) [2.078(4)], Cu2–N8 2.095(4) [2.111(4)], Cu2–N7 2.170(4) [2.232(5)], O1–C30 1.322(6) [1.336(6)], O2–C31 1.337(6) [1.333(5)], C30–C31 1.401(7) [1.407(7)], O2···O3 2.546(5) [2.604(6)], Cu1···Cu2 4.439(1) [4.478(1)]; O1-Cu1-N1 164.1(2) [166.1(2)], O1-Cu1-O2 84.7(2) [85.0(2)], N1-Cu1-O2 100.9(2) [100.3(2)], O1-Cu1-N3 90.2(2) [89.8(2)], N1-Cu1-N3 82.4(2) [82.8(2)], O2-Cu1-N3 172.1(2) [169.2(2)], O1-Cu1-N4 92.9(2) [90.7(2)], N1-Cu1-N4 100.2(2) [100.0(2)], O2-Cu1-N4 102.8(2) [106.3(2)], N3-Cu1-N4 83.5(2) [83.2(2)], O3-Cu2-N6 177.0(2) [178.3(2)], O3-Cu2-N2 99.5(2) [98.1(2)], N6-Cu2-N2 83.1(2) [83.6(2)], O3-Cu2-N8 91.5(2) [93.6(2)], N6-Cu2-N8 85.7(2) [85.2(2)], N2-Cu2-N8 125.2(2) [130.1(2)], O3-Cu2-N7 94.8(2) [95.2(2)], N6-Cu2-N7 86.1(2) [84.5(2)], N2-Cu2-N7 104.1(2) [101.6(2)], N8-Cu2-N7 128.4(2) [125.5(2)].

basically the same in both **5** and **6**. In each case, the TCC is coordinated in a bidentate chelating fashion to only one of the copper ions. It is further linked via one (**6**) or even two (**5**) hydrogen bridges to water molecules bound to the adjacent second metal ion [d(O1···O3) = 2.614(4) Å and d(O1···O4) = 2.994(4) Å in **5**, d(O2···O3) = 2.546(5)/2.604(6) Å in **6**]. The remaining H atoms of these water molecules could be located in hydrogen bridges to perchlorate counteranions [d(O3···O14$_{ClO_4}$) = 2.885 Å and d(O4···O17$_{ClO_4}$) = 2.960 Å in **5**, d(O3···O17$_{ClO_4}$) = 3.050/2.815 Å in **6**]. In **5**·$(ClO_4)_2$, one of these ClO_4^- ions additionally occupies a Jahn–Teller-elongated axial coordination site of Cu2 (see Figure 10). The second proton of the $TCCH_2$ substrate mimic is captured by a side-arm N-donor of the primary ligand scaffold (N6 in **5**, N5 in **6**), which thereby becomes protonated and dissociates from the respective copper ion. The N-bound proton could be located forming a hydrogen bridge to one of the catecholate oxygens [d(N6···O2) = 2.655 Å in **5**, d(N···O) = 2.814 Å in one of the two independent molecules of **6** (not shown in Figure 11)] or to one of the perchlorate counteranions [d(N5···O15$_{ClO_4}$) = 2.899 in the second independent molecule of **6**]. The characteristic C–C and C–O bond lengths of the coordinated TCC clearly identify the dianionic catecholate nature of the substrate mimic, since these bond lengths are diagnostic of the ligand oxidation state[23, 24] (i.e., whether it exists in the catecholate, semiquinone, or quinone state): d(C21–C22) = 1.412(5) Å, d(C21–O1) = 1.339(4) Å, and d(C22–O2) = 1.344(4) Å in **5**; d(C30–C31) = 1.401(7)/1.407(7) Å, d(C30–O1) = 1.322(6)/1.336(6) Å, and d(C31–O2) = 1.337(6)/1.333(5) Å in **6** (values for both independent molecules in the unit cell). This is further corroborated by the lack of any isotropic EPR signals that were to be expected for a semiquinone radical.

Based on the structural findings for **5** and **6**, it seems likely that such binding of the catechol substrate to only one of the two copper ions is one of the reasons for the catecholase activity being lower in the case of the dicopper systems **3** and **4**, that is, in those dicopper complexes that feature increased metal–metal separations due to the constraints of the short ligand side arms. To ensure that the TCC binding mode observed in **5** and **6** is not due to the particular protonation state and to the resulting H-bonding pattern that stems from partial dissociation of the N-donor ligand side arms, a further dicopper-TCC adduct of $[L^3]^-$ was prepared by a different procedure. In this case, a yellow dicopper(I) complex[25] that was prepared at low temperature from HL^3, one equivalent of KO*t*Bu, and two equivalents of $[Cu(NCMe)_4]PF_6$ was treated in situ with one equivalent of the strongly oxidizing tetrachloro-*o*-quinone (TCQ); this caused immediate formation of a green dicopper(II) compound that could be obtained in crystalline form from EtCN/light petroleum (Scheme 5). This complex **7**·PF_6^- was analyzed by X-ray crystallography, and the molecular structure of the cation is depicted in Figure 12.

In **7**, which had evidently been formed in an internal two-electron redox reaction between the copper(I) and the TCQ, the dianionic TCC is again bound to only one of the copper ions (Cu2) in a bidentate chelating fashion and forms a hydrogen bridge to a water molecule located at the adjacent Cu1. Contrary to the situation in **5**, all ligand-side-arm

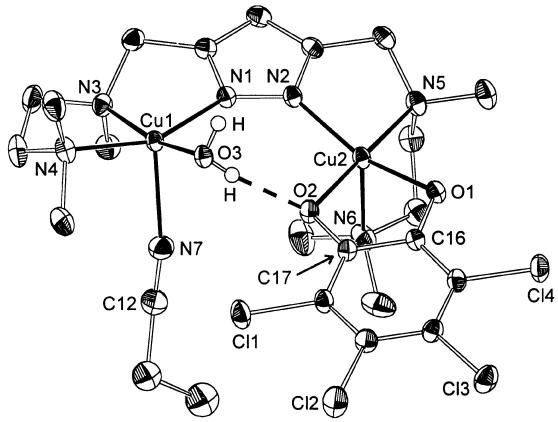

Figure 12. Molecular Structure of **7** (40% probability ellipsoids). All hydrogen atoms except the N- and O-bound hydrogen atoms have been omitted for clarity. Selected atom distances [Å] and bond angles [°]: Cu1–O3 1.963(2), Cu1–N1 1.973(2), Cu1–N3 2.054(2), Cu1–N4 2.057(2), Cu1–N7 2.265(2), Cu2–O2 1.9465(17), Cu2–O1 1.9684(17), Cu2–N2 1.969(2), Cu2–N5 2.091(2), Cu2–N6 2.331(2), O2···O3 2.586(3), O1–C16 1.333(3), O2–C17 1.328(3), C16–C17 1.421(3), Cu1···Cu2 4.288(1); O3-Cu1-N1 95.76(8), O3-Cu1-N3 168.12(8), N1-Cu1-N3 81.33(8), O3-Cu1-N4 93.41(8), N1-Cu1-N4 157.42(9), N3-Cu1-N4 85.47(9), O3-Cu1-N7 93.44(9), N1-Cu1-N7 104.26(9), N3-Cu1-N7 98.44(9), N4-Cu1-N7 95.72(9), O2-Cu2-O1 84.90(7), O2-Cu2-N2 97.34(7), O1-Cu2-N2 158.38(8), O2-Cu2-N5 176.87(8), O1-Cu2-N5 96.56(8), N2-Cu2-N5 82.33(8), O2-Cu2-N6 93.82(8), O1-Cu2-N6 97.10(8), N2-Cu2-N6 104.18(9), N5-Cu2-N6 83.27(8).

N-donors remain coordinated in **7**, and the coordination sphere of Cu1 is completed by an EtCN solvent molecule instead of a second water. By neglecting the different solvent molecules bound to the Cu1 atoms in their Jahn–Teller elongated axial coordination sites, complex **7** can be regarded as the deprotonated form, that is, the corresponding base of **5**. Its molecular structure again confirms that, for the present systems (bearing short ligand side arms), binding to only one of the copper atoms is the preferred coordination mode of the TCC substrate mimic, irrespective of the overall protonation state.

Conclusion

A series of closely related yet distinct dicopper(II) complexes has been synthesized and structurally characterized. One major difference between the four complexes is the individual metal–metal separation that is enforced by the particular pyrazolate-based ligand scaffold: it ranges from 3.45 Å in **2**·$(ClO_4)_4$ to 4.53 Å in **4**·$(ClO_4)_2$. All complexes mediate the catecholase test reaction, albeit with very different activities, which decrease in the order **2**·$(ClO_4)_4$ > **1**·$(ClO_4)_2$ > **3**·$(ClO_4)_2$ ≫ **4**·$(ClO_4)_2$. In all cases the reaction rate is first order in catalyst concentration, in accordance with the idea that two adjacent copper ions are required to accomplish the two-electron substrate oxidation in a cooperative manner. It appears as if there is a correlation between the observed order of catecholase activity and the differences in Cu···Cu distances enforced within the individual catalyst complexes. However, additional effects are certainly in operation, and the minimal activity of **4**·$(ClO_4)_2$ may also stem from its lower redox potential and from the higher coordination number of the two copper ions within the ligand coordination pockets.

 © WILEY-VCH Verlag GmbH, 69451 Weinheim, Germany, 2002 0947-6539/02/0801-0254 $ 17.50+.50/0 *Chem. Eur. J.* **2002**, *8*, No. 1

The most active catecholase model systems **2** and **1** have six-membered chelate rings due to the longer ligand side arms, and thus the coordination sphere of the copper ions is particularly flexible and conformationally relaxed. This is in contrast to previous results for some other model systems, in which a strained chelate situation and a strong distortion from square-pyramidal coordination geometry of the copper ions turned out to be advantageous for catechol oxidation.[12] It is interesting to note that complex **2**·$(ClO_4)_4$ is considerably more active than complex **1**·$(ClO_4)_2$, despite their Cu···Cu distances and their first Cu coordination spheres being very similar. The differences should thus be traced to the higher overall charge of **2** and to the presence of the additional acidic NH functions in close proximity to the bimetallic core. The latter might possibly support proton transfer to (and from) the substrate during turnover—such an effect is strongly reminiscent of the important roles that protein residues play within the active site of natural metalloenzymes.

The structures of "L^3Cu_2" and "L^4Cu_2" with the TCC-substrate analogue suggest a bidentate substrate coordination to only one of the copper ions for those catalysts that feature short ligand side arms and correspondingly larger metal–metal separations; this possibly contributes to the lower activity of these systems. Substrate binding is supported by several H-bonding interactions to water molecules at the adjacent copper or to ligand-side-arm N-donors; this emphasizes the importance of functional groups in proximity to the bimetallic active site. Saturation behavior for the rate dependence on substrate concentration was observed only in two cases, that is, for the most active **2**·$(ClO_4)_4$ and for the least active **4**·$(ClO_4)_2$, whereas a catalytic rate almost independent of substrate concentration (within the range studied) was observed for **1**·$(ClO_4)_2$ and **3**·$(ClO_4)_2$. While the reasons for these differences remain unknown at the present stage, the findings indicate that different rate-determining steps or even distinct mechanisms might well be valid for the individual systems. This underlines the fact that even within a series of closely related compounds every single system has to be studied in detail for a comprehensive understanding.

It is reasonable to assume formation of a dicopper(II) peroxo complex from the reaction of O_2 with the reduced dicopper(I) species generated during the catecholase catalytic cycle. One such peroxo complex stabilized in a tetracopper array of two L^3Cu_2 units was recently isolated and characterized structurally.[25] Detection of H_2O_2 as the product of O_2 reduction in the catecholase reaction of **1**·$(ClO_4)_2$, **2**·$(ClO_4)_4$, and **3**·$(ClO_4)_2$ now suggests that these peroxo complexes liberate H_2O_2 prior to conversion of a further substrate molecule, and a mechanism as outlined in Scheme 6 may be proposed.

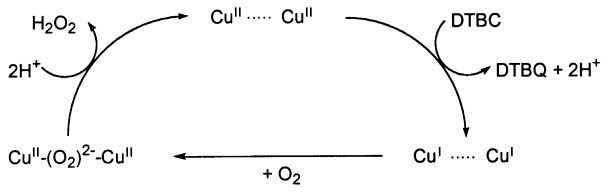

Scheme 6. Proposed mechanism for catechol oxidation by the present complexes.

Further investigations are currently underway to corroborate the mechanistic proposal for the present catalyst systems. It is anticipated that studies on dicopper complexes of a related series of pyrazolate-based ligands that feature side arms of differing lengths (similar to HL^1–HL^4) but with pyridyl N-donors[26] will give further insights into the distinct effects of electronic versus steric tuning on the catecholase activity of such highly preorganized dicopper model systems.

Experimental Section

General Procedures and Methods: The preparation of all complexes was carried out in air. Solvents were dried according to established procedures. All ligands were synthesized according to the reported methods.[14] Microanalyses: Mikroanalytische Laboratorien des Organisch-Chemischen Instituts der Universität Heidelberg. IR spectra: Perkin–Elmer 983 G, recorded as KBr pellets. MS spectra: Finnigan MAT 8230 (FAB-MS), Finnigan TSQ 700 (ESI-MS). UV/Vis spectra: Varian Cary 1E (methanol solution), Perkin Elmer Lambda 19 (diffuse reflectance). Cyclic voltammetry: PAR equipment, (potentiostat/galvanostat 273), in 0.1 M NBu_4PF_6/MeCN. Potentials in V on glassy carbon electrode, referenced to SCE at ambient temperature.

Caution! Although no problems were encountered in this work, transition metal perchlorate complexes are potentially explosive and should be handled with proper precautions.

Complex 1·$(ClO_4)_2$: A solution of HL^1 (325 mg, 1.00 mmol) in MeOH (150 mL) was treated with two equivalents of KO*t*Bu and two equivalents of $Cu(ClO_4)_2 \cdot 6H_2O$ and stirred at room temperature for 1 h. After filtration, all volatile material was evaporated under reduced pressure, then the residue redissolved in methanol and filtered again. The solution was layered with diethyl ether to gradually give green crystals of the product **1**·$(ClO_4)_2$. Yield: 143 mg (0.20 mmol, 20 %); IR (KBr): $\tilde{\nu} = 3541$ (m), 2893 (m), 1626 (w), 1471 (s), 1311 (m), 1257 (w), 1093 (vs), 987 (s), 949 (s), 826 (s), 622 (vs) cm^{-1}; MS (FAB, nibeol): *m*/*z* (%): 548 (28, $[L^1Cu_2(ClO_4)]^+$), 449 (100, $[L^1Cu_2]^+$); elemental analysis calcd for $C_{19}H_{44}Cu_2Cl_2N_6O_{11}$ (730.59): C 31.24, H 6.07, N 11.50; found C 30.98, H 5.76, N 11.91. For X-ray crystallographic characterization, single crystals of the analogous complex **1′**·$(ClO_4)_2$, which has ethanol instead of methanol ligands bound to both copper ions, were obtained from ethanol/diethyl ether.

Complexes 2·$(ClO_4)_4$ and 2·$(BF_4)_4$: A solution of HL^2 (467 mg, 1.00 mmol) in MeOH (150 mL) was treated with two equivalents of $Cu(ClO_4)_2 \cdot 6H_2O$ and stirred at room temperature for 1 h. After filtration all volatile material was evaporated under reduced pressure, the residue redissolved in methanol and filtered again. The solution was layered with diethyl ether to gradually afford the dark green product **2**·$(ClO_4)_4$. Yield: 232 mg (0.23 mmol, 23 %); IR (KBr): $\tilde{\nu} = 3588$ (s), 3130 (m), 2927 (m), 1624 (w), 1469 (s), 1309 (w), 1094 (vs), 952 (m), 805 (w), 623 (vs) cm^{-1}; MS (FAB, nibeol): *m*/*z* (%) 789 (18, $[L^2Cu_2(ClO_4)_2]^+$), 690 (37, $[L^2Cu_2(ClO_4)]^+$), 591 (100, $[L^2Cu_2]^+$), 532 (71, $[L^2Cu_2–HN(Me_2)CH_2]^+$), 504 (83, $[L^2Cu_2 – HN(Me_2)(CH_2)_3]^+$); elemental analysis calcd for $C_{25}H_{56}Cl_4Cu_2N_8O_{17}$ (1009.66): C 29.74, H 5.59, N 11.10; found C 28.91, H 5.75, N 10.67. Complex **2**·$(BF_4)_4$ was prepared by an analogous procedure, by starting from $Cu(BF_4)_2 \cdot 6H_2O$ and using MeCN as the solvent. Single crystals of **2**·$(BF_4)_4$·MeCN were obtained by layering a MeCN solution with diethyl ether. IR (KBr): $\tilde{\nu} = 3212$ (s), 2990 (m), 2888 (m), 2298 (w), 2255 (m), 1472 (s), 1312 (m), 1062 (vs), 956 (m), 821 (m), 809 (m), 766 (m), 520 (s) cm^{-1}; MS (FAB, nibeol): *m*/*z* (%) 789 (36, $[L^2Cu_2F(BF_4)]^+$), 629 (40, $[L^2Cu_2F_2]^+$), 610 (100, $[L^2Cu_2F]^+$), 591 (82, $[L^2Cu_2]^+$), 532 (28, $[L^2Cu_2 – HN(Me_2)CH_2]^+$), 504 (34, $[L^2Cu_2 – HN(Me_2)(CH_2)_3]^+$); elemental analysis calcd for $C_{27}H_{59}B_4Cu_2F_{16}N_9O$ (1000.12): C 32.43, H 5.95, N 12.60, B 4.32, F 30.39; found C 32.22, H 5.79, N 12.76, B 4.21, F 30.30.

Complex 3·$(ClO_4)_2$: A solution of HL^3 (296 mg, 1.00 mmol) in MeOH (150 mL) was treated with two equivalents of KO*t*Bu and two equivalents of $Cu(ClO_4)_2 \cdot 6H_2O$. The solution was stirred at room temperature for 1 h, while CO_2 was bubbled gently into it. After filtration, all volatile material

was evaporated under reduced pressure, the residue was then redissolved in methanol and filtered again. The solution was layered with diethyl ether to gradually afford blue crystals of the product **3**·$(ClO_4)_2$. Yield: 259 mg (0.34 mmol, 34 %); IR (KBr): $\tilde{\nu}$ = 3533 (s), 2929 (s), 1612 (s), 1461 (s), 1395 (s), 1345 (s), 1312 (s), 1286 (m), 1257 (m), 1096 (vs), 943 (s), 846 (s), 810 (m), 775 (m), 622 (s) cm^{-1}; MS (FAB, nibeol): *m/z* (%) 619 (5, $[L^3Cu_2(ClO_4)_2]^+$), 595 (16, $[L^3Cu_2(ClO_4)(CH_3O\text{-}CO_2)]^+$), 551 (12, $[L^3Cu_2(ClO_4)(CH_3O)]^+$), 520 (31, $[L^3Cu_2(ClO_4)]^+$), 421 (100, $[L^4Cu_2]^+$); elemental analysis calcd for $C_{19}H_{42}Cl_2Cu_2N_6O_{13}$ (760.57): C 30.00, H 5.57, N 11.05; found C 29.22, H 4.81, N 11.57.

Complex 4·$(ClO_4)_2$: A solution of HL^4 (523 mg, 1.00 mmol) in MeOH (150 mL) was treated with two equivalents of KO*t*Bu and two equivalents of $Cu(ClO_4)_2 \cdot 6H_2O$, then stirred at room temperature for 1 h. After filtration all volatile material was evaporated under reduced pressure, and the residue was redissolved in methanol and filtered again. The solution was layered with diethyl ether to gradually give light green crystals of the product **4**·$(ClO_4)_2$. Yield: 300 mg (0.33 mmol, 34 %); IR (KBr): $\tilde{\nu}$ = 3415 (s), 2972 (s), 2942 (s), 2881 (m), 1621 (w), 1468 (s), 1379 (m), 1324 (m), 1259 (m), 1087 (vs), 733 (m), 805 (w), 623 (s) cm^{-1}; MS (FAB, nibeol): *m/z* (%): 894 (32, $[L^4Cu_2(ClO_4)_2(OHOCH_3)+1]^+$), 794 (15, $[L^4Cu_2(ClO_4)(OHOCH_3)]^+$), 647 (94, $[L^4Cu_2]^+$); 585 (41, $[L^4Cu+1]^+$), 370 (100, $[L^4Cu-N(CH_2CH_2NEt_2)_2]^+$), 308 (53, $[L^4-N(CH_2CH_2NEt_2)_2+1]^+$); elemental analysis calcd for $C_{29}H_{64}Cl_2Cu_2N_8O_{10}$ (882.865): C 39.45, H 7.31, N 12.69; found C 39.63, H 7.40, N 12.25

Complex 5·$(ClO_4)_2$: A solution of HL^3 (148 mg, 0.50 mmol) in MeOH (150 mL) was treated with KO*t*Bu (150 mg, 1.34 mmol) and two equivalents of $Cu(ClO_4)_2 \cdot 6H_2O$. The solution was stirred at room temperature for 1 h while CO_2 was bubbled gently into it. Then one equivalent of tetrachlorocatechol was added. After filtration, all volatile material was evaporated under reduced pressure, the residue was then redissolved in acetone and filtered again. The solution was layered with light petroleum to gradually afford blue crystals of the product **6**·$(ClO_4)_2$. Yield: 87 mg (0.09 mmol, 18 %); IR (KBr): $\tilde{\nu}$ = 3415 (s), 2921 (m), 1583 (w), 1446 (s), 1370 (w), 1312 (w), 1250 (m), 1086 (vs), 969 (w), 805 (m), 626 (s) cm^{-1}; MS (FAB, nibeol): *m/z* (%): 520 (23, $[L^4Cu_2(ClO_4)]^+$), 421 (75, $[L^4Cu_2]^+$), 257 (100, $[L^4Cu-Me_2N(CH_2)_2NMe]^+$); elemental analysis calcd for $C_{21}H_{36}Cl_6Cu_2N_6O_{12}$·acetone (962.44): C 29.95, H 4.40, N 8.73; found C 30.18, H 4.49, N 8.71.

Complex 6·$(ClO_4)_2$: A solution of HL^4 (262 mg, 0.50 mmol) in MeOH (150 mL) was treated with KO*t*Bu (150 mg, 1.34 mmol) and two equivalents of $Cu(ClO_4)_2 \cdot 6H_2O$, and stirred at room temperature for 1 h. Then one equivalent of tetrachlorocatechol was added. After filtering off the white residue, all the volatile material was evaporated under reduced pressure, and the residue was then taken up in acetone and filtered. The solution was layered with light petroleum to gradually give green crystals of the product **5**·$(ClO_4)_2$. Yield: 43 mg (0.04 mmol, 8 %); IR (KBr): $\tilde{\nu}$ = 3441 (s), 2970 (s), 2929 (s), 2874 (s), 1701 (w), 1635 (w), 1571 (w), 1521 (w), 1444 (s), 1371 (s), 1328 (m), 1255 (m), 1218 (w), 1182 (m), 1088 (s), 968 (s), 927 (w), 826 (w), 806 (s), 787 (s), 733 (m), 682 (w), 622 (s) cm^{-1}; MS (ESI, acetone): *m/z* (%): 893 (1, $[L^4Cu_2C_6Cl_4O_2]^+$), 648 (100, $[L^4Cu_2H]^+$); elemental analysis calcd for $C_{35}H_{64}Cl_6Cu_2N_8O_{11}$ (1112.74): C 37.78, H 5.80, N 10.07; found C 36.95, H 5.63, N 9.66.

Complex 7·PF_6: A stirred solution of HL^3 (115 mg, 0.39 mmol) in EtCN (150 mL) was cooled to −70 °C and treated with one equivalent of KO*t*Bu. Two equivalents of $[Cu(NCMe)_4]PF_6$ were added, and the reaction mixture was stirred for 30 min. One equivalent of *o*-chloranil was added to the yellow solution; this caused it to turn green. After warming the solution to room temperature, stirring was continued for 10 min before the solution was filtered and layered with light petroleum to gradually give green crystals of the product **7**·(PF_6). Yield: 13 mg (0.02 mmol, 4 %); IR (KBr): $\tilde{\nu}$ = 3636 (m), 3570 (m), 3417 (m), 2985 (s), 2926 (s), 1631 (w), 1587 (w), 1529 (m), 1510 (w), 1438 (s), 1371 (s), 1327 (w), 1312 (m), 1291 (w), 1248 (s), 1175 (w), 1160 (w), 1091 (w), 1068 (w), 1036 (m), 1024 (m), 997 (s), 981 (s), 958 (m), 944 (m), 840 (s), 802 (s), 785 (s), 737 (w), 681 (w), 591 (w), 555 (s) cm^{-1}; MS (ESI, acetone): *m/z* (%): 667 (9, $[L^3Cu_2C_6Cl_4O_2]^+$), 421 (100, $[L^3Cu_2]^+$); elemental analysis calcd for $C_{24}H_{38}Cl_4Cu_2F_6N_7O_3P$ (904.48): C 32.52, H 4.32, N 11.06; found C 31.24, H 4.54, N 10.50.

Kinetics of 3,5-di-*tert*-butylcatechol oxidation: The catecholase activity of complexes **1**·$(ClO_4)_2$, **2**·$(ClO_4)_4$, **3**·$(ClO_4)_2$ and **4**·$(ClO_4)_2$ was monitored by UV/Vis spectroscopy by the growth of the absorption band at 400 nm from the product 3,5-DTBQ. The catalytic activity of the complexes was determined by the method of initial rates. In a first test series, concentrations in the range of 2×10^{-6} M to 10^{-5} M were prepared for **1**·$(ClO_4)_2$ and **2**·$(ClO_4)_4$ at a constant concentration of 10^{-3} M of 3,5-DTBC. The concentration of **3**·$(ClO_4)_2$ and **4**·$(ClO_4)_2$ was varied between 5×10^{-6} M and 2×10^{-5} M. In another test series, the complex concentrations were held constant at 10^{-5} M and the catechol substrate was varied in the range of 10^{-4}–10^{-3} M for **1**·$(ClO_4)_2$, **2**·$(ClO_4)_4$ and **3**·$(ClO_4)_2$ and 2×10^{-4}–2×10^{-3} M for **4**·$(ClO_4)_2$. The rate-law dependence of the complex concentration was found to be linear, while for substrate dependence a saturation kinetics was observed in the case of **2**·$(ClO_4)_4$ and **4**·$(ClO_4)_2$. A Michaelis–Menten analysis of the latter data was applied and v_{max}, K_M, and k_{cat} determined from a Lineweaver–Burke plot. All errors were calculated conservatively.

Experiments for the detection of hydrogen peroxide formation: For the detection of H_2O_2, a 10^{-5} M solution of complexes **1**·$(ClO_4)_2$, **2**·$(ClO_4)_4$, **3**·$(ClO_4)_2$, and **4**·$(ClO_4)_2$ was treated with 10^{-3} M 3,5-DTBC. As soon as an absorption of 0.4 was reached, an equal amount of H_2SO_4 (0.005 M) was added to stop the reaction. The reaction mixture was then washed twice with CH_2Cl_2 to remove DTBQ. To a 2 mL aliquot of the aqueous layer a KI solution (1 mL, 0.30 M) was added. Finally, lactoperoxidase was added in catalytic amounts to specifically accelerate the formation of I_3^- in the presence of H_2O_2. The increase of the I_3^- absorption band at 353 nm was monitored by UV/Vis spectroscopy. In order to prove that I_3^- results from the presence of H_2O_2, control experiments were performed starting from a solution of the particular complex (10^{-5} M) and DTBQ (2.4×10^{-4} M) under identical conditions. After adding H_2SO_4 (0.005 M) and washing with CH_2Cl_2 only minor formation of the I_3^- band was observed.

X-ray Crystallography: The measurements were carried out on a Siemens P4 four-circle diffractometer [complex **2**·$(BF_4)_4$], a Nonius Kappa CCD diffractometer [complexes **1′**·$(ClO_4)_2$, **3**·$(ClO_4)_2$, **4**·$(ClO_4)_2$, and **5**·$(ClO_4)_2$], or a Bruker AXS CCD diffractometer [complex **6**·$(ClO_4)_2$ and **7**·(PF_6)] by using graphite-monochromated Mo-K_α radiation. For **2**·$(BF_4)_4$, the intensities of three check reflections (measured every 100 reflections) remained constant throughout the data collection, thus indicating crystal and electronic stability. All calculations were performed by using the SHELXT PLUS software package.[27] The program XPMA[28] was used for graphical handling of the data. For **2**·$(BF_4)_2$, an absorption correction (ψ scan, $\Delta\psi = 10°$) was applied to the data. Atomic coordinates and thermal parameters of the non-hydrogen atoms were refined in fully or partially anisotropic models by full-matrix least-squares calculation based on F^2. In general, the hydrogen atoms were placed at calculated positions and allowed to ride on the atoms they are attached to, or were treated as part of a rigid group (CH_3). In the case of **1′**·$(ClO_4)_2$, the O-bound atoms H1, H2, and H3 were located and refined isotropically. For **2**·$(BF_4)_4$, a CH_3CN solvent molecule was included in the crystal lattice. The O- and N-bound H atoms H1, H70, and H80 were located and refined. Two of the four BF_4^- counteranions were found to be disordered. For **3**·$(ClO_4)_2$, the H4 and H5 atoms of the MeOH molecules were located and refined. In the case of **4**·$(ClO_4)_2$, the H1 atom of the MeO-H-OMe bridge could be located and refined. For **5**·$(ClO_4)_2$, the unit cell contains a partly occupied (0.8) acetone solvent molecule position. All four H atoms bound to the water molecules at Cu1 were located and refined, albeit with moderate temperature factors. The N6-bound H6 atom could be located and refined. In **6**·$(ClO_4)_2$, all H atoms bound to O and N were located and refined. In the case of **7**·(PF_6), the CH2–CH2 link between the N atoms of one ligand side arm and the respective CH_3 groups at the terminal side arm N atom were found to be disordered, as was the ethyl group of the Cu-bound EtCN. H atoms, except those of the disordered atoms, were located in the difference Fourier maps and refined. The cell contains a disordered solvent molecule. Table 4 compiles the data for the structure determinations. Crystallographic data (excluding structure factors) for the structures reported in this paper have been deposited with the Cambridge Crystallographic Data Centre as supplementary publications no. CCDC 161801 [**1′**·$(ClO_4)_2$], 161798 [**2**·$(BF_4)_4$], 161799 [**3**·$(ClO_4)_2$], 161800 [**4**·$(ClO_4)_2$], 161802 [**5**·$(ClO_4)_2$], 161916 [**6**·$(ClO_4)_2$] and 161917 [**7**·(PF_6)]. Copies of the data can be obtained free of charge on application to CCDC, 12 Union Road, Cambridge CB2 1EZ, UK (fax: (+44) 1223-336033; e-mail: deposit@ccdc.cam.ac.uk).

© WILEY-VCH Verlag GmbH, 69451 Weinheim, Germany, 2002
0947-6539/02/0801-0256 $ 17.50+.50/0 *Chem. Eur. J.* **2002**, *8*, No. 1

Table 4. Crystal data and refinement details for the complexes.

	1′·$(ClO_4)_2$	**2**·$(BF_4)_4$	**3**·$(ClO_4)_2$	**4**·$(ClO_4)_2$	**5**·$(ClO_4)_2$	**6**·$(ClO_4)_2$	**7**·PF_6
Formula	$C_{21}H_{48}N_6O_{11}Cl_2Cu_2$	$C_{27}H_{59}B_4Cu_2F_{16}N_9O$ + 1 MeCN	$C_{19}H_{42}Cl_2Cu_2N_6O_{13}$	$C_{31}H_{68}Cl_2Cu_2N_8O_{10}$	$C_{21}H_{36}Cl_6Cu_2N_6O_{12}$ + 0.8 acetone	$C_{35}H_{64}Cl_6Cu_2N_8O_{11}$ + 1 acetone	$C_{24}H_{38}Cl_4Cu_2F_6N_7O_3P$
M [g mol^{-1}]	758.64	1000.15	760.57	910.92	950.80	1170.80	904.48
crystal size [mm]	0.20 × 0.20 × 0.20	0.30 × 0.30 × 0.30	0.10 × 0.20 × 0.25	0.10 × 0.10 × 0.05	0.40 × 0.40 × 0.30	0.38 × 0.26 × 0.17	0.22 × 0.22 × 0.30
crystal system	monoclinic	monoclinic	triclinic	orthorhombic	monoclinic	monoclinic	triclinic
space group	$P2_1/n$	$P2_1$	$P\bar{1}$	$Aba2$	$P2_1/n$	$P2_1$	$P\bar{1}$
a [Å]	10.556(2)	11.412(2)	8.819(2)	13.588(3)	17.366(4)	14.1449(3)	12.4327(6)
b [Å]	25.667(5)	15.634(3)	12.843(3)	25.200(5)	9.574(2)	13.8461(3)	13.1551(7)
c [Å]	12.214(2)	12.076(2)	14.397(3)	12.058(2)	22.737(5)	26.6750(7)	13.7200(7)
α [°]	90.00(0)	90.00(0)	81.99(3)	90.00(0)	90.00(0)	90.00(0)	62.154(1)
β [°]	106.37(3)	102.23(1)	81.04(3)	90.00(0)	91.53(3)	100.64(1)	87.539(1)
γ [°]	90.00(0)	90.00(0)	73.99(3)	90.00(0)	90.00(0)	90.00(0)	73.926(1)
V [Å^3]	3175	2106	1540	4129	3779	5134.5(2)	1896.7(2)
Z	4	2	2	8	4	4	2
$\rho_{calcd.}$ [g cm^{-3}]	1.587	1.577	1.640	1.465	1.671	1.515	1.584
T [K]	200	200	200	200	200	173	190(2)
μ (Mo-K_α) [mm^{-1}]	1.570	1.118	1.623	1.220	1.615	1.204	1.512
hkl range	±13, ±31, ±15	−2–13, ±18, ±14	±10, ±15, ±17	±16, -31–30, ±14	±22, ±11, ±29	±17, ±17, 0–33	±18, -16–19, 0–20
2θ range [°]	3.8–52.0	4.3–50.0	4.2–52.1	3.2–52.0	2.9–55.2	3.0–52.8	4.2–64.1
measured refl.	49484	4068	12020	31611	17100	40021	33357
unique refl. (Rint)	6221 (0.0901)	3918 (0.0229)	6069 (0.0290)	4049 (0.1752)	8582 (0.0476)	20420 (0.0726)	12555 (0.0356)
observed refl. $I > 2\sigma(I)$	4497	3486	4925	2554	5494	15591	9561
refined parameters	399	526	391	235	523	1237	570
resid. electron dens. [eÅ^{-3}]	0.47/−0.38	1.10/−0.82	0.94/−0.56	0.77/−0.36	0.61/−0.32	1.11/−0.55	1.32/−0.72
$R1$	0.037	0.048	0.034	0.061	0.043	0.047	0.043
$wR2$ (refinement on F^2)	0.082	0.130	0.080	0.121	0.124	0.121	0.130
GOF	1.026	1.132	1.037	1.018	0.997	0.984	1.017

Acknowledgement

We are grateful to Prof. Dr. G. Huttner for his generous and continuous support. Dr. Peter Kircher and (the late) Dr. Laszlo Zsolnai are sincerely thanked for collecting some of the crystallographic data. Funding for this work by the Deutsche Forschungsgemeinschaft (Habilitandenstipendium and Heisenbergstipendium to F.M.), by the state of Baden-Württemberg (Landesgraduiertenstipendium to J.A.) and by the Fonds der Chemischen Industrie is gratefully acknowledged.

[1] See for example: K. D. Karlin, *Science* **1993**, *261*, 701–708; S. J. Lippard, J. M. Berg, *Principles of Bioinorganic Chemistry*, University Science Books, CF, **1994**; W. Kaim, B. Schwederski, *Bioanorganische Chemie*, Teubner, Stuttgart, **1991**; *Bioinorganic Catalysis* (Ed.: J. Reedijk), Marcel Dekker, New York, **1993**; M. W. Göbel, *Angew. Chem.* **1994**, *106*, 1201–1203; *Angew. Chem. Int. Ed. Engl.* **1994**, *33*, 1141–1143; N. Sträter, W. N. Lipscomb, T. Klabunde, B. Krebs, *Angew. Chem.* **1996**, *108*, 2158–2191; *Angew. Chem. Int. Ed. Engl.* **1996**, *35*, 2024–2055.

[2] B. J. Wallar, J. D. Lipscomb, *Chem. Rev.* **1996**, *96*, 2625–2657; L. Que, Jr., *J. Chem. Soc. Dalton Trans.* **1997**, 3933–3940; J. Du Bois, T. J. Mizoguchi, S. J. Lippard, *Coord. Chem. Rev.* **2000**, *200–202*, 443–485.

[3] E. I. Solomon, U. M. Sundaram, T. E. Machonkin, *Chem. Rev.* **1996**, *96*, 2563–2605; H.-C. Liang, M. Dahan, K. D. Karlin, *Curr. Opin. Chem. Biol.* **1999**, *3*, 168–175.

[4] K. A. Magnus, H. Ton-That, J. E. Carpenter, *Chem. Rev.* **1994**, *94*, 727–735; N. Kitajima, Y. Moro-oka, *Chem. Rev.* **1994**, *94*, 737–757; K. D. Karlin, S. Kaderli, A. D. Zuberbühler, *Acc. Chem. Res.* **1997**, *30*, 139–147; P. L. Holland, W. B. Tolman, *Coord. Chem. Rev.* **1999**, *190–192*, 855–869; M. Fontecave, J.-L. Pierre, *Coord. Chem. Rev.* **1998**, *170*, 125–140.

[5] W. Kaim, J. Rall, *Angew. Chem.* **1996**, *108*, 47–64; *Angew. Chem. Int. Ed. Engl.* **1996**, *35*, 43–60; A. G. Blackman, W. B. Tolman, *Struct. Bonding* **2000**, *97*, 179–211; H. Decker, R. Dillinger, F. Tuczek, *Angew. Chem.* **2000**, *112*, 1656–1660; *Angew. Chem. Int. Ed.* **2000**, *40*, 1591–1595; S. Schindler, *Eur. J. Inorg. Chem.* **2000**, 2311–2326.

[6] D. E. Wilcox, A. G. Porras, Y. T. Hwang, K. Lerch, M. E. Winkler, E. I. Solomon, *J. Am. Chem. Soc.* **1985**, *107*, 4015–4027; C. Eicken, F. Zippel, K. Buldt-Karentzoloulos, B. Krebs, *FEBS Lett.* **1998**, *436*, 293–299; A. Rompel, H. Fischer, D. Meiwes, K. Buldt-Karentzoloulos, R. Dillinger, F. Tuczek, H. Witzel, B. Krebs, *J. Biol. Inorg. Chem.* **1999**, *4*, 56–63.

[7] T. Klabunde, C. Eicken, J. C. Sacchettini, B. Krebs, *Nature Struct. Biol.* **1998**, *5*, 1084–1090; C. Eicken, B. Krebs, J. C. Sacchettini, *Curr. Opin. Struct. Biol.* **1999**, *9*, 677–683.

[8] A. B. P. Lever, B. S. Ramaswamy, S. R. Pickens, *Inorg. Chim. Acta* **1980**, *46*, L59–61; T. R. Demmin, M. D. Swerdloff, M. M. Rogic, *J. Am. Chem. Soc.* **1981**, *103*, 5795–5804; D. Bolus, G. S. Vigee, *Inorg. Chim. Acta* **1982**, *67*, 19–25; G. Speier, *J. Mol. Cat.* **1986**, *37*, 259–267; M. Réglier, C. Jorand, B. Waegell, *J. Chem. Soc. Chem. Commun.* **1990**, 1752–1755; J.-P. Chyn, F. L. Urbach, *Inorg. Chim. Acta* **1991**, *189*, 157–163; M. R. Malachowski, L. J. Tomlinson, M. G. Davidson, M. J. Hall, *J. Coord. Chem.* **1992**, *25*, 171–174; D. A. Rockcliffe, A. E. Martell, *J. Mol. Catal. A* **1995**, *99*, 101–114; F. Zippel, F. Ahlers, R. Werner, W. Haase, H.-F. Nolting, B. Krebs, *Inorg. Chem.* **1996**, *35*, 3409–3419; Y.-H. Chung, H.-H. Wei, Y.-H. Liu, G.-H. Lee, Y. Wang, *J. Chem. Soc. Dalton Trans.* **1997**, 2825–2829; J. Manzur, A. M. Garcia, V. Rivas, A. M. Atria, J. Valenzuela, E. Spodine, *Polyhedron* **1997**, *16*, 2299–2305; R. Wegner, M. Gottschaldt, H. Görls, E.-G. Jäger, D. Klemm, *Angew. Chem.* **2000**, *112*, 608–612; *Angew. Chem. Int. Ed. Engl.* **2000**, *39*, 595–599; P. Gentschev, N. Möller, B. Krebs, *Inorg. Chim. Acta* **2000**, *300–302*, 442–452; R. Wegner, M. Gottschaldt, H. Görls, E.-G. Jäger, D. Klemm, *Chem. Eur. J.* **2001**, *7*, 2143–2157.

[9] M. R. Malachowski, H. B. Huynh, L. J. Tomlinson, R. S. Kelly, J. W. Furbee, Jr., *J. Chem. Soc. Dalton Trans.* **1995**, 31–36.

[10] N. Oishi, Y. Nishida, K. Ida, S. Kida, *Bull. Chem. Soc. Jpn.* **1980**, *53*, 2847–2850; U. Casellato, S. Tamburini, P. A. Vigato, A. de Stefani, M. Vidali, D. E. Fenton, *Inorg. Chim. Acta* **1983**, *69*, 45–51; M. R. Malachowski, M. G. Davidson, *Inorg. Chim. Acta* **1989**, *162*, 199–204; C.-H. Kao, H.-H. Wie, Y.-H. Liu, G.-H. Lee, Y. Wang, C.-J. Lee, *J. Inorg. Biochem.* **2001**, *84*, 171–178.

[11] K. D. Karlin, Y. Guiltneh, T. Nicholson, J. Zubieta, *Inorg. Chem.* **1985**, *24*, 3725–3727; H. Börzel, P. Comba, H. Pritzkow, *Chem. Commun.* **2001**, 97–98.

[12] J. Reim, B. Krebs, *J. Chem. Soc. Dalton Trans.* **1997**, 3793–3804.

[13] E. Monzani, L. Quinti, A. Perotti, L. Casella, M. Gullotti, L. Randacchio, S. Geremia, G. Nardin, P. Faleschini, G. Tabbi, *Inorg. Chem.* **1998**, *37*, 553–562; E. Monzani, G. Battaini, A. Perotti, L. Casella, M. Gullotti, L. Santagostini, G. Nardin, L. Randacchio, S. Geremia, P. Zanello, G. Opromolla, *Inorg. Chem.* **1999**, *38*, 5359–5369.

[14] F. Meyer S. Beyreuther, K. Heinze, L. Zsolnai, *Chem. Ber./Recueil* **1997**, *130*, 605–613; F. Meyer, U. Ruschewitz, P. Schober, B. Antelmann, L. Zsolnai, *J. Chem. Soc. Dalton Trans.* **1998**, 1181–1186.

[15] F. Meyer, K. Heinze, B. Nuber, L. Zsolnai, *J. Chem. Soc. Dalton Trans.* **1998**, 207–213; F. Meyer, P. Rutsch, *Chem. Commun.* **1998**, 1037–1038; F. Meyer, E. Kaifer, P. Kircher, K. Heinze, H. Pritzkow, *Chem. Eur. J.* **1999**, *5*, 1617–1630.

[16] A. W. Addison, T. N. Rao, J. Reedijk, J. van Rijn, G. C. Verschoor, *J. Chem. Soc. Dalton Trans.* **1984**, 1349–1356.

[17] M. Duggan, N. Ray, B. Hathaway, G. Tomlinson, P. Brint, K. Pelin, *J. Chem. Soc. Dalton Trans.* **1980**, 1342–1348.

[18] L. Casella, O. Carugo, M. Gullotti, S. Garofani, P. Zanello, *Inorg. Chem.* **1993**, *32*, 2056–2067.

[19] R. R. Gagné, R. P. Kreh, J. A. Dodge, *J. Am. Chem. Soc.* **1979**, *101*, 6917–6927.

[20] For redox potentials of the catechol substrates see: L. Horner, E. Geyer, *Chem. Ber.* **1965**, *98*, 2016–2045; M. D. Stallings, M. M. Morrison, D. T. Sawyer, *Inorg. Chem.* **1981**, *20*, 2655–2660; S. Harmalker, S. E. Jones, D. T. Sawyer, *Inorg. Chem.* **1983**, *22*, 2790–2794; J. Rall, M. Wanner, M. Albrecht, F. M. Hornung, W. Kaim, *Chem. Eur. J.* **1999**, *5*, 2802–2808. Cyclic voltammetry performed during this study gives the following values for the quinone/semiquinone couple ($E_{1/2}$ in V vs. SCE, MeCN solution, 0.1 M $N(n\text{-}Bu)_4PF_6$, 200 mV s^{-1}): 3,5-di-*tert*-butyl-*o*-benzoquinone -0.55, tetrachloro-*o*-benzoquinone $+0.13$.

[21] J. Tokunaga, *J. Chem. Eng. Data* **1975**, *20*, 41–46.

[22] H. Jenzer, W. Jones, H. Kohler, *J. Biol. Chem.* **1986**, *261*, 15550–15556.

[23] L. M. Berreau, S. Mahapatra, J. A. Halfen, R. P. Houser, V. G. Young, Jr., W. B. Tolman, *Angew. Chem.* **1999**, *111*, 180–183; *Angew. Chem. Int. Ed.* **1999**, *38*, 207–210.

[24] M. Pascaly, M. Duda, F. Schweppe, K. Zurlinden, F. K. Müller, B. Krebs, *J. Chem. Soc. Dalton Trans.* **2001**, 828–837; W. O. Koch, V. Schünemann, M. Gerdan, A. X. Trautwein, H.-J. Krüger, *Chem. Eur. J.* **1998**, *4*, 1255–1265.

[25] The reaction of this dicopper(I) species with O_2 gave rise to a structurally characterized tetracopper(II)-peroxo complex: F. Meyer, H. Pritzkow, *Angew. Chem.* **2000**, *112*, 2199–2202; *Angew. Chem. Int. Ed.* **2000**, *39*, 2112–2115.

[26] J. Ackermann, F. Meyer, H. Pritzkow, unpublished results.

[27] G. M. Sheldrick, *SHELXL-97, Program for Crystal Structure Refinement*, Universität Göttingen, **1997**; *SHELXS-97, Program for Crystal Structure Solution*, Universität Göttingen, **1997**; G. M. Sheldrick, *SHELXTL 5.1*, Bruker AXS, Madison, Wisconsin, USA.

[28] L. Zsolnai, G. Huttner, *XPMA*, Universität Heidelberg, **1998**; http://www.rzuser.uni-heidelberg.de/~v54/xpm.html.

Received: June 27, 2001 [F3374]

 © WILEY-VCH Verlag GmbH, 69451 Weinheim, Germany, 2002 0947-6539/02/0801-0258 $ 17.50+.50/0